Nanoscale

COMMUNICATION

View Article Online
View Journal | View Issue

Cite this: *Nanoscale*, 2014, **6**, 9545

Received 24th January 2014
Accepted 6th June 2014

DOI: 10.1039/c4nr00479e

www.rsc.org/nanoscale

A highly conducting graphene film with dual-side molecular n-doping†

Youngsoo Kim,‡[ab] Jaesung Park,‡[cd] Junmo Kang,[e] Je Min Yoo,[a] Kyoungjun Choi,[a] Eun Sun Kim,[a] Jae-Boong Choi,[e] Chanyong Hwang,[c] K. S. Novoselov[d] and Byung Hee Hong*[a]

Doping is an efficient way to engineer the conductivity and the work function of graphene, which is, however, limited to wet-chemical doping or metal deposition particularly for n-doping, Here, we report a simple method of modulating the electrical conductivity of graphene by dual-side molecular n-doping with diethylenetriamine (DETA) on the top and amine-functionalized self-assembled monolayers (SAMs) at the bottom. The resulting charge carrier density of graphene is as high as -1.7×10^{13} cm^{-2}, and the sheet resistance is as low as $\sim 86 \pm 39\ \Omega$ sq^{-1}, which is believed to be the lowest sheet resistance of monolayer graphene reported so far. This facile dual-side n-doping strategy would be very useful to optimize the performance of various graphene-based electronic devices.

Introduction

Graphene is an atom-thick material with honeycomb lattice structures consisting of sp^2 bonded carbons,[1] which has been intensively studied owing to its fascinating 2-dimensional properties including flexibility,[2] ultrahigh mobility,[3] high transparency[4] and outstanding heat dissipating ability[5] useful for various electronic and optoelectronic applications.[6] Among these properties, the electrical tunability based on its unusual band structure[1] enables the optimization of the electrical conductivity and the work-function of graphene, which is important for various conducting electrode applications.[7] Doping is one of the efficient methods to control the electrical properties of graphene, and several doping strategies have been devised, including substitutional doping,[8,9] molecular adsorption,[10–14] covalent functionaliztion,[15–18] substrate surface modification[19–23] and the use of metallic thin films or nanoparticles.[24–26,39,40]

However, the doping strength of these doping methods is limited by insufficient charge-transfer from dopants and by electron scattering from substituted atoms leading to low carrier mobility and conductivity. Previously, the chemical doping of graphene has been mainly carried out by coating graphene with dopants or transferring graphene on dopant layers. For example, self-assembled monolayers (SAMs) have been utilized as ultrathin and uniform graphene-doping layers functionalized on an oxide surface,[22,26] which are advantageous because of their simple fabrication process applicable to various surface and interface engineering.[22,27–29] However, the SAM doping on a single-side of graphene did not provide enough doping strength to improve the electrical conductivity of graphene. As the amount of transferred charge is proportional to the surface area of graphene in contact with dopants, simultaneous doping on the dual-side of graphene would be more efficient to enhance the electrical properties of graphene. Here, we demonstrate a simple method to tune the electrical properties of graphene synthesized by chemical vapor deposition (CVD) with dual-side chemical doping – the bottom-side doping *via* substrate modification with NH_2-SAMs and the top-side doping with diethylenetriamine (DETA) molecules.

Results and discussion

To investigate the electrical properties of the doped graphene, we prepared four different types of graphene field effect transistor samples – top-side, bottom-side and dual-side n-doped graphene and the pristine graphene. Fig. 1 shows the schematic views of three types of n-doped graphene devices. To obtain the bottom-side n-doped graphene, NH_2-SAMs were constructed on the surface of the SiO_2 (100 nm)/Si substrate by dipping in the

[a]*Department of Chemistry, Seoul National University, 1 Gwanak-ro, Seoul 151-742, Korea. E-mail: byunghee@snu.ac.kr*

[b]*Department of Physics & Astronomy, Seoul National University, 1 Gwanak-ro, Seoul 151-742, Korea*

[c]*Center for Nanometrology, Korea Research Institute of Standards and Science, Gajeong-Ro, Daejeon 305-340, Korea*

[d]*School of Physics and Astronomy, University of Manchester, M13 9PL Manchester, UK*

[e]*Sungkyunkwan Advanced Institute of Nanotechnology (SAINT), Sungkyunkwan University, Seobu-ro, Suwon 440-746, Korea*

† Electronic supplementary information (ESI) available. See DOI: 10.1039/c4nr00479e

‡ These authors contributed equally to this work.

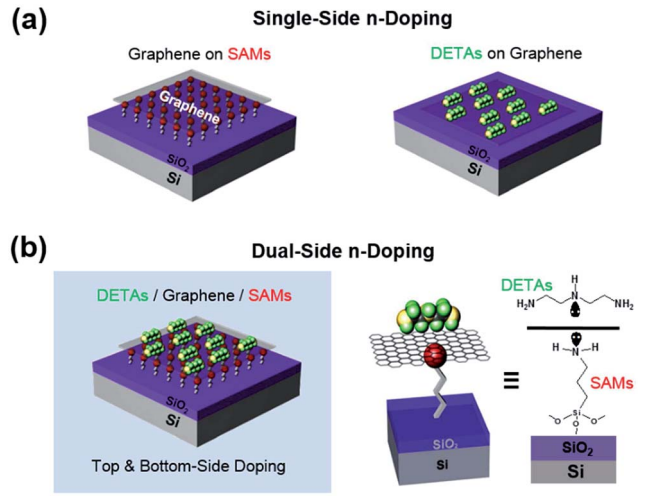

Fig. 1 Schematic views of three different types of n-doped graphene. (a) Single-side doped graphene: top-side n-doping (left) with evaporated DETA molecules and bottom-side n-doping (right) with amine-functionalized SAMs. (b) Dual-side doped graphene (left) and graphical representation of the molecular structure of the dopants on the both sides of graphene (right).

aqueous solution of 3-aminopropyltriethoxysilane (volume ratio of 500 : 1) for 30 minutes. The NH_2-SAM modified substrate was dried by blowing with a nitrogen gun, followed by the careful transfer of graphene onto the substrate. Diethylenetriamine (DETA) was used as the top-side n-doping molecule, which exhibits a strong n-doping effect.[12] Vapor-phase DETA doping was carried out in a sealed Petri-dish from the droplet on tissue under 70 °C baking on a hot plate for 30 minutes. Thus, the dual-side doping with DETA/NH_2-SAMs was completed as shown in Fig. 1b, where the two types of dopants including the lone pair electrons of amine functional groups are efficiently positioned to maximize the electron doping effect on both sides of graphene.

Fig. 2a shows the Raman spectra of the pristine, single-side, and dual-side doped graphene with NH_2-SAMs and DETA. The G band of graphene was up-shifted from 1585 cm^{-1} (pristine) to 1588 cm^{-1} (NH_2-SAM modified) and 1590 cm^{-1} (DETA doped) and 1600 cm^{-1} (DETA/NH_2-SAM modified) due to the effect of the Fermi level shift on the phonon frequencies as a result of electron doping.[30]

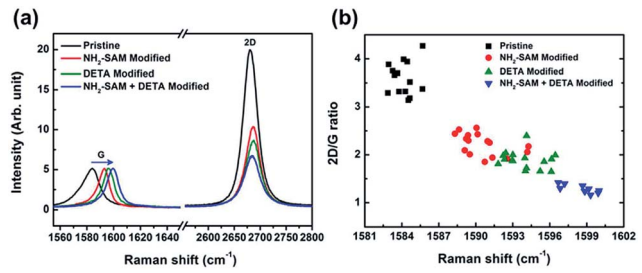

Fig. 2 (a) The representative Raman spectra of graphene with different dopants (pristine, NH_2-SAMs, DETA and DETA/NH_2-SAMs). (b) Raman shift *vs.* $I_{(2D)}/I_{(G)}$ ratio plot of pristine, NH_2-SAM modified, DETA doped, and dual-side modified (DETA/NH_2-SAMs) graphene.

Noticeably, the intensity ratio of $I_{(2D)}/I_{(G)}$ also decreased from 3.6 ± 0.3 to 2.2 ± 0.2 for the DETA doped graphene, 1.9 ± 0.2 for the NH_2-SAM doped graphene, and 1.3 ± 0.1 for dual-side modified graphene (Fig. 2b) with the up-shift of the G band when chemical doping was applied. This blue shift of the G band and the decreased ratio of $I_{(2D)}/I_{(G)}$ exhibit characteristics of typical electron doping of graphene, which has been shown in previous reports.[30–32] Therefore, we confirmed that our doping process successfully induced strong n-doping of graphene.

In Fig. 3b, the graphene field effect transistors show different charge neutral points with respect to different doping conditions (schematic shown in Fig. 3a). Initially, the charge neutral point (V_{CNP}) of pristine graphene transistors starting at 2 V was negatively changed to −40 V in the bottom-side doped graphene device with NH_2-SAMs. The point was shifted more down to −68 V in the dual-side doped graphene devices modified with DETA/NH_2-SAMs on the both sides of graphene films. The charge neutral point of graphene devices was also shifted to −48 V after top-side doping with DETA (Fig. 3c). The mobility of graphene devices can be extracted from the following equation:

$$\mu = \frac{1}{C_i}\frac{d\sigma}{dV_G}$$

where C_i is the capacitance of 100 nm SiO_2 (3.24×10^{-8} F cm^{-2}), σ is the conductivity of graphene, and V_G is the applied gate voltage.

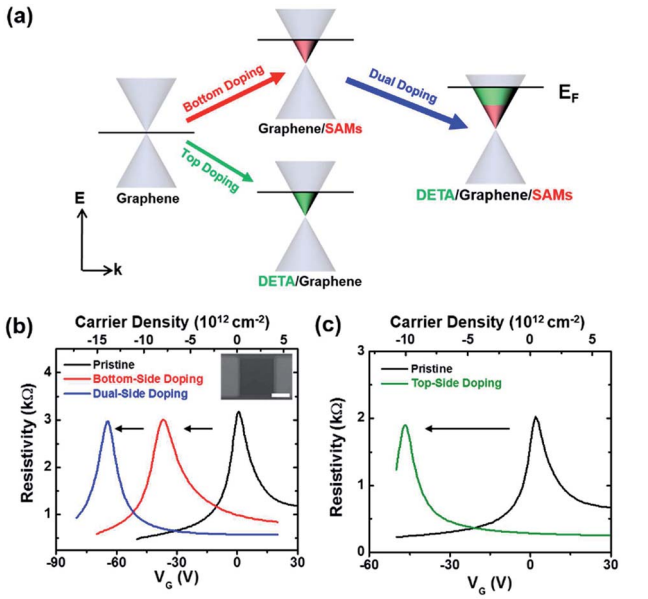

Fig. 3 (a) Schematic illustration of the Fermi energy level (E_f) diagram of different types of n-doped graphene. All the doping processes (bottom-side, top-side and dual-side n-doping) induce a significant up-shift of E_f, in particular, dual-side n-doped graphene has much stronger n-type behavior from the molecular n-doping of bottom-side and top-side. (b) Current–gate voltage transfer characteristics of the graphene FETs on pristine, bottom-side, and dual-side doped graphene. The inset shows the SEM image of graphene FETs with 100 μm scale bar. (c) Current–gate voltage transfer characteristics of the graphene FETs with pristine and DETA doped graphene.

Graphene field effect devices show relatively high mobility considering their scales (length: 50–250 μm, width: 250 μm) although the graphene channels possibly include some defects such as grain boundaries, ripples and small cracks.[33,34] While the pristine graphene device shows 2791 $cm^2\ V^{-1}\ s^{-1}$ for the hole region and 2125 $cm^2\ V^{-1}\ s^{-1}$ for the electron region, the NH_2-SAM modified graphene devices show 1660 $cm^2\ V^{-1}\ s^{-1}$ for the electron region and 751 $cm^2\ V^{-1}\ s^{-1}$ for the hole region. Such discordant tendency between the electron and hole mobility of the NH_2-SAM device was mainly caused by misalignment between electrodes and graphene channels in terms of work-function.[35] It is supposed that the suppression in mobility originates from the inhomogeneous coverage of NH_2-SAMs, leading to charge impurities on graphene channels.[36]

However, after applying DETA on the top-side of the NH_2-modified graphene device, its hole and electron mobility changed to 1775 $cm^2\ V^{-1}\ s^{-1}$ and 1808 $cm^2\ V^{-1}\ s^{-1}$, respectively. These increased mobilities can be explained by the screening effect of charged impurities.[37,38] The top-side doped device with DETA showed 2598 $cm^2\ V^{-1}\ s^{-1}$ and 2426 $cm^2\ V^{-1}\ s^{-1}$ for hole and electron regions, respectively. In Fig. 3c, the schematic diagram represents the tuning of the Fermi level by the chemical doping process. Both bottom-side doping with NH_2-SAM and top-side doping with DETA induced the up-shift of the Fermi level in the case of intrinsic graphene. Interestingly, the dual-side doping resulted in a further increased Fermi level, showing a much stronger n-doping effect than single-side doping.

To confirm the average molecular doping effect at room temperature, dozens of graphene field effect transistors were measured. The results are plotted as a function of carrier density and the charge neutral point in Fig. 4a and b. Carrier density is estimated by a typical equation, $n = -\alpha(V_G - V_{CNP})$, with $\alpha = 2.16 \times 10^{11}\ cm^{-2}\ V^{-1}$. We found that the carrier density of graphene was tunable up to $-1.7 \times 10^{13}\ cm^{-2}$ by using dual-side doping, which is the highest value among the recent reports on n-doping of graphene.[23,27,39] To further examine the doping characteristics induced by each dopant, we also measured the sheet resistance of pristine and doped graphene on SiO_2 (100 nm)/Si substrates. The results from more than 30 different positions of graphene are shown in Fig. 4c and d. The sheet resistance of graphene gradually decreased from $923 \pm 148\ \Omega\ sq^{-1}$, $385 \pm 140\ \Omega\ sq^{-1}$, $150 \pm 77\ \Omega\ sq^{-1}$ and to $86 \pm 39\ \Omega\ sq^{-1}$, respectively for pristine, NH_2-SAMs, DETA, and dual-side doped graphene. These results correspond well with the shifts of charge neutral points in the graphene field effect devices, implying that the charge transfer between molecules and graphene can be maximized by increasing the surface area of graphene in contact with n-dopants. The transmittance of dual-side doped graphene measured at 550 nm wavelength is ~96% (Fig. S1†).

To demonstrate the doping stability, we measured the sheet resistance of the dual-side n-doped graphene after air exposure, thermal heating, and light exposure. The results show that the average sheet resistance was increased by ~20% after 60 min air exposure. After 15 min heating at 70 °C and 100 °C, the sheet resistance increased to 150 and 350 Ohm sq^{-1}, respectively (see details in Fig. S2†). In addition, the FET characteristics of DETA-doped graphene with respect to doping time and temperature were also examined (Fig. S3†).

Finally, we fabricated transparent heaters based on n-doped graphene. Fig. 5 depicts the time-dependent temperature profiles of the graphene-based heaters treated with different dopants. As previously reported, the steady state temperature of the heater depends on the sheet resistance of graphene films.[43] As a result, the dual-side doped graphene heater exhibits a heating temperature as high as 54 °C, while single-side doped

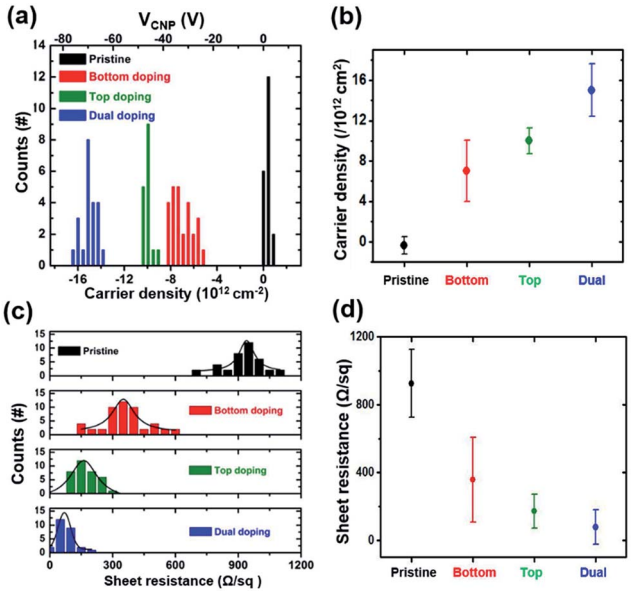

Fig. 4 (a) Histogram of charge neutral points of graphene FETs doped by NH_2-SAMs, DETA and DETA/NH_2-SAMs (dual-side doped). (b) Averages and distributions of the carrier density plot of four different types of graphene FETs. (c) Histogram of the sheet resistance of graphene doped by NH_2-SAMs, DETA and DETA/NH_2-SAMs (dual-side doped). (d) Averages and distributions of the sheet resistance plot of four different types of graphene FETs.

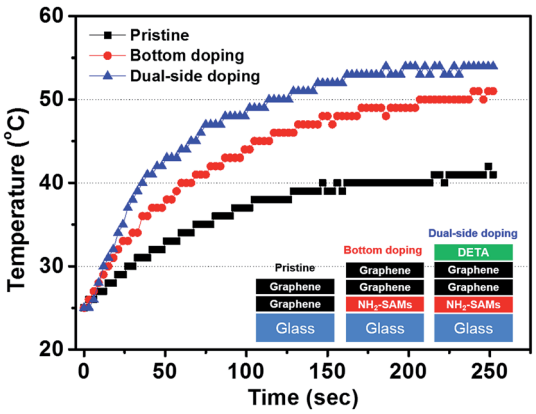

Fig. 5 The temperature profiles of pristine, bottom doped and dual-side doped graphene heaters. The size of the heaters was 1.8 × 1.8 cm^2. The temperature responses of the heaters were monitored every three seconds using an infrared camera. The 20 V of input voltage was supplied to the heaters through two-terminal side copper electrodes.

and pristine graphene heaters show ~51 °C and ~40 °C, respectively (Fig. S4†).

Conclusion

In conclusion, we have developed a simple and efficient dual-side molecular doping method for graphene, demonstrating effective work function modulation, high carrier density (-1.7×10^{13} cm^{-2}) and significant reduction of sheet resistance (86 ± 39 Ω sq^{-1}), which is believed to be the best conductivity for large-area CVD graphene so far. The actual performance of the dual-side doped graphene film was confirmed by fabricating a transparent heater that exhibits higher heating temperature compared to single-side doped or undoped graphene films. We expect that further efforts to optimize the dual-side doping method would enable a wide variety of practical applications of graphene films that require low sheet resistance comparable to indium tin oxide (ITO) as well as high transparency and flexibility useful for flexible electronics in the future.[6,12,22,40–43]

Experimental

Sample preparation

The graphene film is synthesized on 25 μm thick copper foil by CVD methods, using a mixture of CH_4 (50 sccm) and H_2 (5 sccm) gas as a source with vacuum pumping at 1000 °C. The transfer process of graphene is followed by the conventional process: PMMA is spin-coated on top of graphene and then copper foil etched with ammonium persulfate solution (20 mM with distilled water). Highly P-doped Si substrate covered with SiO_2 of 100 nm thickness is used for electrical measurement of graphene field effect devices. Free-standing graphene on distilled water is carefully transferred onto the bare SiO_2/Si and NH_2-SAM modified SiO_2/Si substrate respectively and PMMA is removed by using acetone.

Cr (5 nm) and Au (30 nm) are deposited thermally for the metal contact of the 3-terminal graphene device by using a pre-patterned stencil mask. Graphene channels are isolated using an electron beam lithography technique. To avoid deviation in growth conditions, we use the same graphene sample grown in the same bath. Each device has as large scales as 250 μm width and 50–250 μm length. Before doping the graphene film, thermal annealing is carried out at 300 °C for 1 h in Ar and H_2 gas environments to remove PMMA residues and trapped water after the graphene device fabrication process. For UV-Vis measurement and the graphene heater, the same n-doping method was applied to a transparent substrate (glass). In the case of the graphene heater, 2 layers of graphene were used to obtain uniform heating.

Characterization

The n-type doping characteristics of graphene are defined by micro-Raman spectra using a 1 mW, 514 nm Ar laser with a spot size of 2 μm (Renishaw inVia Raman microscope). The transmittance was measured using a Scinco s-3100 UV-Vis spectrometer. Four types of graphene-based field effect transistors were fabricated to measure the difference of the electrical performances. An Agilent 2602 was used on 3-terminal geometry with source, drain and gate. The voltage of 10 mV was applied between source and drain with the gate voltage sweep (−70 V to 80V). The sheet resistance of graphene (0.2 mm × 0.2 mm square geometry) was measured using a four-point probe with a nanovoltmeter (Keithley 6221, 2182A) based on the van der Pauw method considering

$$R_s = \frac{\pi}{\ln 2}\frac{V}{I}$$

where R_s is the sheet resistance, V is the applied voltage and I is the current. The temperature responses of the heaters were measured using an infrared camera.[43]

Acknowledgements

This work was supported by the Global Research Lab (GRL) Program (2011-0021972), the Global Frontier Research Program (2011-0031627), the Basic Science Research Program (2012M3A7B4049807) and the Nano-Material Technology Development Program (2012M3A7B4049888) through the National Research Foundation of Korea (NRF) funded by the Ministry of Science, ICT and Future Planning, Korea.

Notes and references

1 K. S. Novoselov, A. K. Geim, S. V. Morozov, D. Jiang, Y. Zhang, S. V. Dubonos, I. V. Grigorieva and A. A. Firsov, *Science*, 2004, **306**, 666–669.
2 Y. Lee, S. Bae, H. Jang, S. Jang, S.-E. Zhu, S. H. Sim, Y. I. Song, B. H. Hong and J.-H. Ahn, *Nano Lett.*, 2010, **10**, 490–493.
3 K. I. Bolotin, K. J. Sikes, Z. Jiang, M. Klima, G. Fudenberg, J. Hone, P. Kim and H. L. Stormer, *Solid State Commun.*, 2008, **146**, 351–355.
4 R. R. Nair, P. Blake, A. N. Grigorenko, K. S. Novoselov, T. J. Booth, T. Stauber, N. M. R. Peres and A. K. Geim, *Science*, 2008, **320**, 1308.
5 A. A. Balandin, S. Ghosh, W. Bao, I. Calizo, D. Teweldebrhan, F. Miao and C. N. Lau, *Nano Lett.*, 2008, **8**, 902–907.
6 Q. Bao and K. P. Loh, *ACS Nano*, 2012, **6**, 36773694.
7 S. Bae, H. Kim, Y. Lee, X. Xu, J.-S. Park, Y. Zheng, J. Balakrishnan, T. Lei, H. Ri Kim, Y. I. Song, Y.-J. Kim, K. S. Kim, B. Ozyilmaz, J.-H. Ahn, B. H. Hong and S. Iijima, *Nat. Nanotechnol.*, 2010, **5**, 574–578.
8 L. S. Panchakarla, K. S. Subrahmanyam, S. K. Saha, A. Govindaraj, H. R. Krishnamurthy, U. V. Waghmare and C. N. R. Rao, *Adv. Mater.*, 2009, **21**, 4726–4730.
9 D. Wei, Y. Liu, Y. Wang, H. Zhang, L. Huang and G. Yu, *Nano Lett.*, 2009, **9**, 1752–1758.
10 F. Schedin, A. K. Geim, S. V. Morozov, E. W. Hill, P. Blake, M. I. Katsnelson and K. S. Novoselov, *Nat. Mater.*, 2007, **6**, 652–655.
11 S. Ryu, L. Liu, S. Berciaud, Y.-J. Yu, H. Liu, P. Kim, G. W. Flynn and L. E. Brus, *Nano Lett.*, 2010, **10**, 4944–4951.
12 Y. Kim, J. Ryu, M. Park, E. S. Kim, J. M. Yoo, J. Park, J. H. Kang and B. H. Hong, *ACS Nano*, 2014, **8**, 868–874.

13 Y. Kim, J. M. Yoo, H. Jeon and B. H. Hong, *Phys. Chem. Chem. Phys.*, 2013, **15**, 18353–18356.
14 X. Dong, D. Fu, W. Fang, Y. Shi, P. Chen and L.-J. Li, *Small*, 2009, **5**, 1422–1426.
15 S. Niyogi, E. Bekyarova, M. E. Itkis, H. Zhang, K. Shepperd, J. Hicks, M. Sprinkle, C. Berger, C. N. Lau, W. A. deHeer, E. H. Conrad and R. C. Haddon, *Nano Lett.*, 2010, **10**, 4061–4066.
16 J. M. Englert, C. Dotzer, G. Yang, M. Schmid, C. Papp, J. M. Gottfried, H.-P. Steinrück, E. Spiecker, F. Hauke and A. Hirsch, *Nat. Chem.*, 2011, **3**, 279–286.
17 B. Guo, Q. Liu, E. Chen, H. Zhu, L. Fang and J. R. Gong, *Nano Lett.*, 2010, **10**, 4975–4980.
18 D. Usachov, O. Vilkov, A. Grüneis, D. Haberer, A. Fedorov, V. K. Adamchuk, A. B. Preobrajenski, P. Dudin, A. Barinov, M. Oehzelt, C. Laubschat and D. V. Vyalikh, *Nano Lett.*, 2011, **11**, 5401–5407.
19 D. Wei, Y. Liu, Y. Wang, H. Zhang, L. Huang and G. Yu, *Nano Lett.*, 2009, **9**, 1752–1758.
20 R. Wang, S. Wang, D. Zhang, Z. Li, Y. Fang and X. Qiu, *ACS Nano*, 2010, **5**, 408–412.
21 M. Lafkioti, B. Krauss, T. Lohmann, U. Zschieschang, H. Klauk, K. v. Klitzing and J. H. Smet, *Nano Lett.*, 2010, **10**, 1149–1153.
22 Y. y. Wang, Z. h. Ni, T. Yu, Z. X. Shen, H. m. Wang, Y. h. Wu, W. Chen and A. T. Shen Wee, *J. Phys. Chem. C*, 2008, **112**, 10637–10640.
23 J. Park, W. H. Lee, S. Huh, S. H. Sim, S. B. Kim, K. Cho, B. H. Hong and K. S. Kim, *J. Phys. Chem. Lett.*, 2011, **2**, 841–845.
24 K. M. McCreary, K. Pi and R. K. Kawakami, *Appl. Phys. Lett.*, 2011, **98**, 192101–192103.
25 K. Pi, K. M. McCreary, W. Bao, W. Han, Y. F. Chiang, Y. Li, S. W. Tsai, C. N. Lau and R. K. Kawakami, *Phys. Rev. B: Condens. Matter Mater. Phys.*, 2009, **80**, 075406.
26 J. H. Chen, C. Jang, S. Adam, M. S. Fuhrer, E. D. Williams and M. Ishigami, *Nat. Phys.*, 2008, **4**, 377–381.
27 S. Huh, J. Park, K. S. Kim, B. H. Hong and S. B. Kim, *ACS Nano*, 2011, **5**, 3639–3644.
28 S. A. DiBenedetto, A. Facchetti, M. A. Ratner and T. J. Marks, *Adv. Mater.*, 2009, **21**, 1407–1433.
29 W. H. Lee, J. Park, Y. Kim, K. S. Kim, B. H. Hong and K. Cho, *Adv. Mater.*, 2011, **23**, 3460–3464.
30 A. Das, S. Pisana, B. Chakraborty, S. Piscanec, S. K. Saha, U. V. Waghmare, K. S. Novoselov, H. R. Krishnamurthy, A. K. Geim, A. C. Ferrari and A. K. Sood, *Nat. Nanotechnol.*, 2008, **3**, 210–215.
31 C. Casiraghi, S. Pisana, K. S. Novoselov, A. K. Geim and A. C. Ferrari, *Appl. Phys. Lett.*, 2007, **91**, 233103–233108.
32 C. Stampfer, F. Molitor, D. Graf, K. Ensslin, A. Jungen, C. Hierold and L. Wirtz, *Appl. Phys. Lett.*, 2007, **91**, 241907.
33 Q. Yu, L. A. Jauregui, W. Wu, R. Colby, J. Tian, Z. Su, H. Cao, Z. Liu, D. Pandey, D. Wei, T. F. Chung, P. Peng, N. P. Guisinger, E. A. Stach, J. Bao, S.-S. Pei and Y. P. Chen, *Nat. Mater.*, 2011, **10**, 443–449.
34 P. Y. Huang, C. S. Ruiz-Vargas, A. M. van der Zande, W. S. Whitney, M. P. Levendorf, J. W. Kevek, S. Garg, J. S. Alden, C. J. Hustedt, Y. Zhu, J. Park, P. L. McEuen and D. A. Muller, *Nature*, 2011, **469**, 389–392.
35 D. B. Farmer, R. Golizadeh-Mojarad, V. Perebeinos, Y.-M. Lin, G. S. Tulevski, J. C. Tsang and P. Avouris, *Nano Lett.*, 2008, **9**, 388–392.
36 F. Schedin, A. K. Geim, S. V. Morozov, E. W. Hill, P. Blake, M. I. Katsnelson and K. S. Novoselov, *Nat. Mater.*, 2007, **6**, 652–655.
37 T. Ando, *J. Phys. Soc. Jpn.*, 2006, **75**, 074716–074717.
38 S. Adam, E. H. Hwang, V. M. Galitski and S. Das Sarma, *Proc. Natl. Acad. Sci. U. S. A.*, 2007, **104**, 18392–18397.
39 P.-H. Ho, Y.-C. Yeh, D.-Y. Wang, S.-S. Li, H.-A. Chen, Y.-H. Chung, C.-C. Lin, W.-H. Wang and C.-W. Chen, *ACS Nano*, 2012, **6**, 6215–6221.
40 Z. K. Liu, J. H. Li, Z. H. Sun, G. A. Tai, S. P. Lau and F. Yan, *ACS Nano*, 2012, **6**, 810–818.
41 K. S. Kim, Y. Zhao, H. Jang, S. Y. Lee, J. M. Kim, K. S. Kim, J. H. Ahn, P. Kim, J. Y. Choi and B. H. Hong, *Nature*, 2009, **457**, 706–710.
42 J. Kang, D. Shin, S. Bae and B. H. Hong, *Nanoscale*, 2012, **4**, 5527–5537.
43 J. Kang, H. Kim, K. S. Kim, S.-K. Lee, S. Bae, J.-H. Ahn, Y.-J. Kim, J.-B. Choi and B. H. Hong, *Nano Lett.*, 2011, **11**, 5154–5158.